AAS 17-370

LANDING ON SMALL BODIES TRAJECTORY DESIGN, ROBUST NONLINEAR GUIDANCE AND CONTROL

Eric Joffre[*], Mattia Zamaro[†], Nuno Silva[‡], Andrés Marcos[§], Pedro Simplício[¶] and Barbara Richardson[‖]

While common Descent and Landing strategies involve extended periods of forced motion, significant fuel savings could be achieved by exploiting the natural dynamics in the vicinity of the target. However, small bodies are characterised by perturbed and poorly known dynamics environments, calling for autonomous guidance, navigation and robust control. Airbus Defence and Space and the University of Bristol have been contracted by the UK Space Agency to investigate the optimisation of landing trajectories, including novel approaches from dynamical systems theory, and robust nonlinear control techniques. This paper presents these techniques, with an application to the strategic case of a mission to Phobos.

INTRODUCTION

Space sample return missions have a record of revolutionising planetary science. In 2012, new chemical analyses carried out by the University of Chicago on the lunar material collected by Apollo 14 fifty years earlier brought new elements to the disputed question of the origin of the Moon, casting a new doubt on the most widely accepted *Giant Impact* theory.[1] The US manned missions to the Moon of the Apollo programme were the first missions to return extra-terrestrial samples, then followed by the Soviet Luna missions, relying solely on advanced robotics. Technological advances have recently enabled sample return from farther celestial bodies: NASA's Stardust mission returned cometary dust in 2006, JAXA's Hayabusa mission returned microscopic grains of asteroid material in 2010 and NASA recently launched the OSIRIS-REx mission to collect a sample from the Bennu asteroid, with the objective to return it to Earth in 2023. Among the future candidates for exploration missions are the low-gravity and irregularly-shaped Martian moons. In particular, Phobos as a destination is receiving significant attention from the international community both for the wide scientific interest to finally solve the unknowns surrounding the nature of its formation, and because such a precursor mission could represent the technology drive to test some of the key components for a future international Mars Sample Return mission. The results of the analysis on Earth of a sample from Phobos will also characterise the exploitable in-situ resources, possibly enabling to use the moon as a waypoint for the future human exploration of the Martian System.

[*]Mission Analysis and AOCS/GNC Engineer, AOCS/GNC and Flight Dynamics UK R&D coordinator, Airbus Defence and Space Ltd, Gunnels Wood Road, Stevenage SG1 2AS, UK
[†]Mission Analysis and AOCS/GNC Engineer, AOCS analyst, contractor for Airbus Defence and Space Ltd
[‡]Head of AOCS/GNC and Flight Dynamics UK, Airbus Defence and Space Ltd
[§]Head of TASC Technology for AeroSpace Control, Senior Lecturer, University of Bristol, Queen's Building, University Walk, Bristol BS8 1TR, UK
[¶]PhD Researcher in Aerospace Engineering, University of Bristol
[‖]National Space Technology Programme Manager, UKSA, Polaris House, North Star Avenue, Swindon SN2 1SZ, UK

Close proximity operations including descent and landing are some of the most critical phases for sample return missions, typically characterised by very challenging propellant consumption requirements. While common descent strategies involve an extended period of forced motion, either by translating to the surface from a close hovering station-keeping point or by starting the descent from a distant quasi-satellite orbit, significant fuel savings could be achieved by further exploiting the natural dynamics in the vicinity of the target. However, a common characteristic of the gravitational environments around asteroids and small bodies like Phobos is that they are both highly perturbed and essentially poorly known, calling for the development of reliable autonomous guidance, navigation and robust control strategies.

As prime contractor for the European Space Agency's *Phobos Sample Return* Phase A study, Airbus Defence and Space Ltd has been working towards the definition and preliminary design of a Phobos Sample Return spacecraft and mission, including orbital transfers, proximity operations, up to Earth re-entry trajectories. In parallel to this ESA system study, Airbus Defence and Space has been awarded a grant by the UK Space Agency to specifically investigate innovative strategies for the design and optimisation of the landing trajectories, as well as robust nonlinear guidance and control techniques. Started in April 2016, this one year project brings together Airbus Defence and Space industrial experience in systems design, mission analysis and GNC with the University of Bristol leading-edge research in the frame of autonomous systems and robust control.

After briefly summarising the history and current baseline for a sample return mission from Phobos, the paper will describe the dynamics environment considered for the study and the specific challenges associated with the descent and landing on small bodies. In the following section, novel approaches for the selection and optimisation of propellant efficient landing trajectories will be introduced and compared to more classical strategies. Confronted to the reality of a highly perturbed and unknown dynamics environment, the last part of the paper will introduce the investigation of robust closed-loop guidance and control schemes. While aiming at proposing a generic guidance and control framework for the descent and landing on small bodies, the paper will focus on Phobos as a strategic and archetypal study case, illustrating the implications of the proposed strategy on the operations for a future interplanetary Sample Return mission.

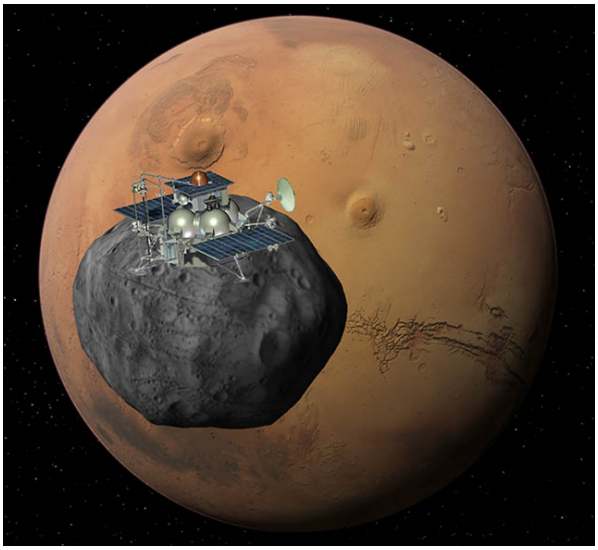

Figure 1. Artist's view of a lander on Phobos

PHOBOS SAMPLE RETURN MISSION AND ASSOCIATED CONSTRAINTS

Airbus Defence and Space heritage on landing and sample return missions

Landing and sample return missions to the Moon, asteroids, Mars and its moons have been studied for many years by Airbus Defence and Space. Following the successful launch and subsequent mission of Rosetta towards Comet 67P/Churyumov-Gerasimenko, some of the recent system studies conducted by Airbus Defence and Space for the European Space Agency include the following:

- The Mars Precision Lander (MPL)[2] system study investigated the safe landing of a Sample Fetch Rover, as part of the Mars Sample Return (MSR) programme. This rover would retrieve the sample cache obtained by the future NASA/ESA sample caching rover and place it in the Mars Ascent Vehicle (MAV) for the first stage of its journey back to Earth.
- Marco Polo and Marco Polo-R[3] were M-class candidate missions of ESA Cosmic Vision Science Programme, with the objective to bring a 100 g sample including dust and centimetre-size pebbles back to Earth for analysis. Both landing for surface operations and a much swifter *touch-and-go* strategies were studied for the collection of the samples.
- The Mars Moon Sample Return (MMSR) mission was initially studied by ESA in the Agency's Concurrent Design Facility (CDF), in the frame of the Mars Robotic Exploration Programme. It was the precursor for the industrial pre-Phase A Phootprint, whose primary objective and first mission requirement was to return approximately 100 g of loose material from Phobos.[4]
- In the continuity of Phootprint, Airbus Defence and Space Ltd led a 12 months Phase A Phobos Sample Return (PhSR) study, that was completed and delivered at the end of 2016, and that will be presented in further detail in the next paragraph.

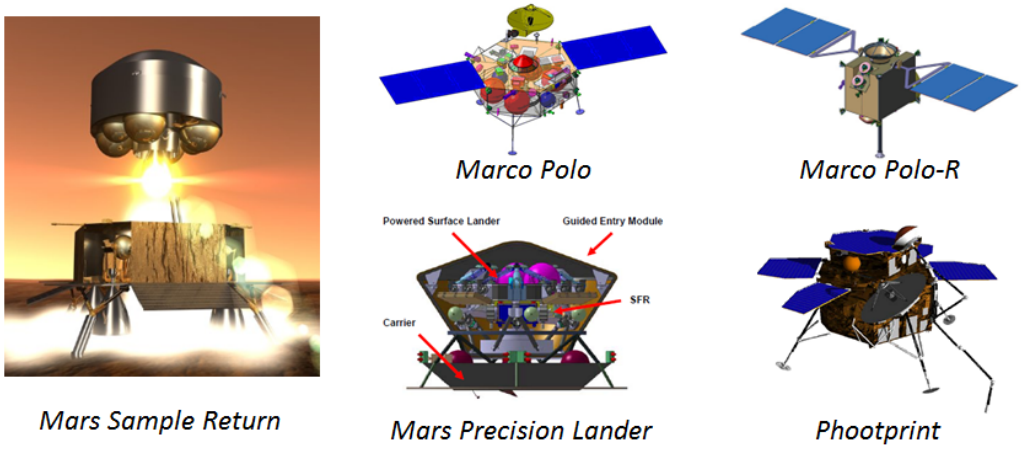

Figure 2. Airbus DS involvement in landing and sample return system studies, proposed concepts

These projects have involved multidisciplinary teams of engineers in comprehensive system studies, thus providing a deep understanding of the constraints associated with the major subsystems for such missions, and in particular: the touch-down and landing system, the sample handling system, the Earth Re-entry Capsule (ERC), and the Guidance Navigation and Control (GNC) for proximity operations, which is the object of the UKSA-funded study presented in this paper.

Phobos Sample Return mission overview and specific requirements for landing

The Phobos Sample Return Phase A study is the continuation of the Phootprint pre-phase A, conducted by Airbus Defence and Space in 2014, with the renewed high-level objective to bring back 100 g of the moon surface regolith back to Earth for analysis. Reference mission scenarios and associated spacecraft designs have been baselined for the mission, including a joint ESA-Roscosmos scenario, with a Proton-M* launch from Baikonour in 2024 (baseline) or 2026 (backup), followed by an interplanetary transfer of about 11 months, and an ESA standalone scenario, with an Ariane 5 ECA* launch from Kourou in 2024/2025 (baseline) or 2026 (backup), followed by an interplanetary transfer of about 2 years. After a Mars Orbit Insertion (MOI) bringing the spacecraft into a highly elliptical orbit, a sequence of manoeuvres puts PhSR on a Quasi-Satellite Orbit† (QSO) around *Deimos* for a first science phase to characterise Mars's smaller moon, orbiting the planet at about 20,000 km. Then, manoeuvres are performed to reach a *Phobos* QSO, for a new characterisation phase aimed at identifying the preferred landing sites. After a minimum of 3 fly-by trajectories for high resolution measurements of potential landing sites at low altitudes (typically 5 km), and a first rehearsal to ensure equipments are operating nominally, the descent is initiated via a hovering point about 10 km above the surface of Phobos, for communication and navigation purposes. On Phobos's surface, images of the site are communicated to Earth for the selection of the samples, then collected by means of a robotic arm. Following Phobos ascent and return transfer, the Earth Re-entry Capsule (ERC) containing the samples is set to land in either Kazakhstan or Australia.

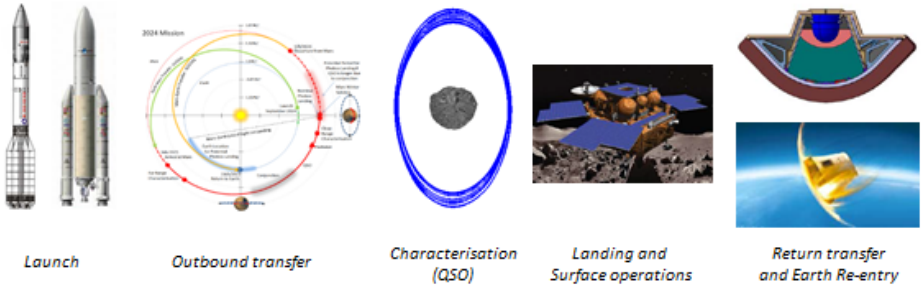

Figure 3. Phobos Sample Return main mission phases

The work presented in this paper investigates alternative landing strategies that take further advantage of the natural dynamics in the vicinity of the small body. Specific requirements applicable to the landing include the following:

- 20% accessibility of Phobos surface (goal is 50%), including latitudes up to 60 deg
- landing accuracy on Phobos better than 50 m at a 95 % confidence level
- landing velocities at Phobos: vertical < 1.5 m/s, horizontal < 1 m/s
- final free-fall (without using thrusters) of 20 m, to avoid surface contamination

*subject to launchers continued availability, the Angara-5 and Ariane 64 Launch Vehicles being planned to progressively replace Proton and Ariane 5 ECA respectively, at dates that are not presently known.

†In a three-body problem, Quasi-Satellite Orbits, also known as Distant Retrograde Orbits (DROs) are 1:1 resonant orbits with the smaller primary, lying outside its Hill sphere but remaining in its vicinity following ellipse-like relative trajectories. Achieved by a small eccentricity of the orbit around the main primary with a semi-major axis similar to the smaller primary, they are still slightly perturbed by the attraction of the latter and known to be unstable in the long-term.

MISSION ANALYSIS AND REFERENCE LANDING TRAJECTORY DESIGN

The objective of this section is to describe the dynamics environment applicable for the study, the models used for the simulations, and the derivation of reference open-loop landing trajectories.

Dynamics in the vicinity of Phobos and reference frames

Mars largest moon Phobos is a small body with dimensions 13.1 km $\times$ 11.1 km $\times$ 9.3 km (mean ellipsoid), orbiting the Red Planet at a mean altitude of less than 6,000 km and a period of about 7 hours and 40 minutes*. The next table provides some physical constants and orbital parameters† used in the study, both for Mars (orbit around the Sun) and Phobos[5] (orbit around Mars).

Table 1. Main physical properties and orbital parameters used for Mars and Phobos

Body	Gravity μ_g $(m^3 s^{-2})$	Mass (kg)	Semi-major axis (km)	Eccentricity	Inclination (deg)
Mars	4.2828×10^{13}	6.4185×10^{23}	227.9478×10^{6}	0.0934	0.0323
Phobos	711200	1.0659×10^{16}	9379.2557	0.0156	0.0186

Given the low value for Phobos' orbit eccentricity, the first level of approximation for the dynamics of a spacecraft in the Mars-Phobos system is described by the *Circular Restricted Three Body Problem* (CRTBP):[6] even though this model is simplified, it gives some insight into the main characteristics of the dynamics. In particular, given the reduced mass ratio of $m_{\text{Phobos}}/(m_{\text{Mars}}+m_{\text{Phobos}}) = 1.65 \times 10^{-8}$, and the dimensions of Phobos, the L1 and L2 collinear Libration Points of the Mars-Phobos system lie only a few kilometers (about 3.5 km) above the surface of the moon. An important consequence of this property is that there is no possibility for a Keplerian orbit around Phobos, and the third-body perturbation of Mars gravity cannot be neglected for the design and simulation of descent and landing trajectories‡. The next figure shows the location of the L1 and L2 Lagrangian points assuming a CRTBP model, together with the (in-plane) *zero-velocity curves* associated with their corresponding levels of Jacobi Integral.[6]

The dominant perturbations to this model are the *ellipticity* of Phobos' orbit around Mars, and the *non-spherical gravitational field* of Phobos[7,8] : owing to its high inhomogeneity and very irregular shape, the gravity field of the moon cannot be described properly by a spherical (Keplerian) potential. Using spherical coordinates r for the radius, θ for the co-latitude, and ϕ for the longitude, and a reference radius R, the gravity potential is described by a spherical harmonics double expansion:

$$U_g(r,\theta,\phi) = \frac{\mu_{g_{\text{Phobos}}}}{R} \sum_{n=0}^{\infty} \left(\frac{R}{r}\right)^{n+1} \sum_{m=0}^{n} C_n^m(\phi) P_n^m(\cos(\theta)) \tag{1}$$

$$\text{where:} \quad \begin{cases} C_n^m(\phi) &= C_{n,m}\cos(m\phi) + S_{n,m}\sin(m\phi) \\ P_n^m(x) &= \left(1-x^2\right)^{m/2} \dfrac{d^m}{dx^m} P_n(x) \\ P_n(x) &= \dfrac{1}{2^n n!} \dfrac{d^n}{dx^n}\left(x^2-1\right)^n \end{cases} \tag{2}$$

*shorter than the Mars rotation period: an observer on Mars would see Phobos rise in the West and set in the East.

†Source: NASA JPL ephemeris at epoch 25 July 2012 00.00 UTC

‡This property, very specific to the Mars-Phobos system, will generally not be observed in the vicinity of another small body, and in particular for an asteroid. Not only thought to be strategic for application in a future Phobos Sample Return mission, the Phobos study case has been selected as a challenging dynamical system capturing all the nonlinearity of a three body problem, to test the robustness and performance of the landing guidance and control.

The next figure illustrates the location of the CRTBP L1 and L2 Lagrangian points, and provides the Gravity Harmonics coefficients $C_{n,m}$ and $S_{n,m}$ for a reference radius of $R = 11$ km.[9]

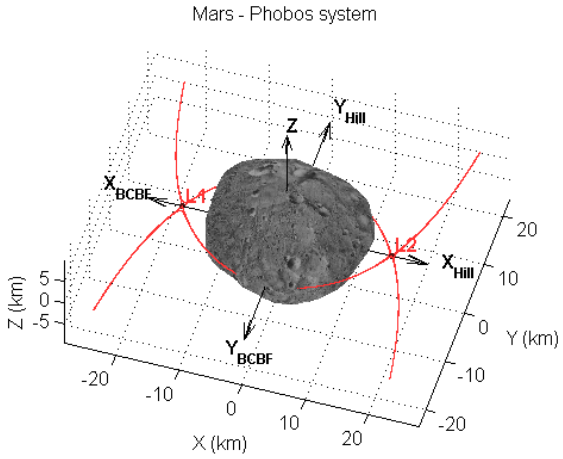

(n,m)	$C_{n,m}$	$S_{n,m}$
(2,0)	-0.04698	0
(2,1)	0.00136	0.00138
(2,2)	0.02276	-0.000202
(3,0)	0.00293	0
(3,1)	-0.00309	0.00181
(3,2)	-0.00847	-0.000655
(3,3)	0.00224	-0.01392
(4,0)	0.00762	0
(4,1)	0.00347	-0.000776
(4,2)	-0.00288	-0.00112
(4,3)	-0.0028	0.00337
(4,4)	-0.0012	-0.000622

Figure 4. Phobos reference frames, CRTBP Lagrangian Points L1, L2 and associated in-plane zero-velocity curves (left), gravity harmonics coefficients[9] (right)

Mars non-spherical gravitational perturbation, and in particular its first zonal coefficient J_2 due to the planet's oblateness, also has a non-negligible contribution, but it remains one order of magnitude below the aforementioned perturbations for the application considered.

The previous figure also illustrates the reference frames used in the study:

- The Hill frame has its origin at the moon's barycentre and rotates with a fixed attitude with respect to its orbit around Mars: the vertical z-axis is perpendicular to the orbital plane, and the radial x-axis is pointing outwards from the Mars-Phobos barycentre. This is the usual frame considered for the description of the motion in a three-body problem.
- The Body-Centred Body-Fixed frame (BCBF) also has its origin at the moon's barycentre but its attitude is fixed with respect to the body's geometry: the vertical z-axis is aligned along the body's spin axis, and the x-axis is pointing towards the intersection of a body's reference Prime Meridian and the equatorial plane.

As a long-term effect of Mars' gravity gradient (tidal force), Phobos has the interesting property that its revolution around Mars and rotation around its spin axis are synchronous, and almost non-tilted: Phobos is said to be *tidally locked*, like our Moon, always showing the same face to the planet. With this approximation, Hill and BCBF frames z-axes are coincident, while their x-axes differ only by the definition of the Prime Meridian. In particular, Phobos' Prime Meridian is formally identified by the location of the point constantly pointing towards Mars on the body's equator: therefore the two frames differ by a rotation of 180 deg of their x-y plane's axes. In reality, an additional oscillation between a minimum of 0.30 deg and a maximum of 1.90 deg is observed. However the dynamics of this motion, seen from Phobos as a Mars' libration in latitude is much slower (period of 2.26 terrestrial years) than the time-scale of a mission segment around Phobos.[10]

Dynamics models: Mission Analysis and Guidance (MAG) and Dynamics, Kinematics and Environment (DKE)

The BCBF frame is the most natural coordinate system to be used for a landing problem, and will serve as the reference frame for the expression of the equations of motion, as well as all subsequent trajectory representations in the next sections. As the main challenge to be addressed in the context of the study is the derivation of robust closed-loop landing strategies in perturbed and poorly known environments, two different models for the descent and landing have been implemented:

- A first model is considered to represent the dynamics environment that would be used on the ground for the mission analysis, the definition and design of sets of reference landing trajectories. Assumed to be representative enough of the dynamics in flight, this is also the model to be used by the on-board guidance function. Therefore, this model will be referred to as the *Mission Analysis and Guidance* (MAG) model.
- As the dynamics in orbit will differ from the dynamics predicted on the ground, and in order to be able to assess the robustness of closed-loop landing guidance and control, a second model is needed to simulate the *actual* dynamics experienced by the spacecraft. This model will be referred to as the *Dynamics, Kinematics and Environment* (DKE). As the actual dynamics cannot be known exactly, this model is a statistical model with some parameters drawn from predefined probability distributions: each DKE simulation is therefore a single realisation of the statistical model. It also includes second order perturbations such as Mars' J_2 and Mars' libration apparent motion from Phobos's BCBF frame, not included in the MAG model.

Based on the previous description of the various contributors to the orbital dynamics in the vicinity of Phobos, the next table summarises the assumptions considered for each of these models:

Table 2. Difference of assumptions for the MAG and DKE dynamics models

	Dynamics model	
Contributors	MAG	DKE
Mars gravity model	Keplerian (Spherical potential)	Kepler + J_2 (GHs = first zonal coefficient)
BCBF wrt Hill	Fixed and non-tilted (equatorial)	Librating
Phobos gravity model	Full GHs $(m = 4, n = 4)$ Deterministic	Full GHs $(m = 4, n = 4)$ Probabilistic
Probabilistic parameters	None	GHs coefficients $C_{n,m}$ and $S_{n,m}$ $\mathcal{N}(\mu_{\text{MAG}}, \sigma = 100\%\|\mu_{\text{MAG}}\|)$

The equations of motion are fairly complex, to account for all the effects described above, but they can be written in a generic state-space form, with the state vector $\underline{X}$ (BCBF position and velocity), vector field f (MAG or DKE), command matrix B and propulsive acceleration $\underline{U}$, as:

$$\dot{\underline{X}} = f(\underline{X}, t) + B \cdot \underline{U} \tag{3}$$

Due to Phobos' orbit ellipticity, the system is non autonomous and it must be augmented with an equation for Phobos true anomaly ν on its orbit around Mars. This standalone equation can be written as follows, e being Phobos orbit eccentricity and n its mean motion:

$$\dot{\nu} = n\frac{(1 + e\cos(\nu))^2}{(1 - e^2)^{3/2}} \tag{4}$$

Initial guess for landing trajectories using Libration Point Orbits and invariant manifolds

As described in the previous paragraph, it is impossible to design an orbit around Phobos that is not strongly perturbed by the gravity of Mars. Therefore, instead of using distant Quasi-Satellite Orbits (QSOs) for the selection of the landing site, followed by a sequence of costly forced manoeuvres for the descent and landing, the solution investigated in this study consists in using Libration Point Orbits (LPOs) as natural close observation platforms, and their invariant manifolds, initiated by a small magnitude ΔV on the LPO, as an *initial guess* for a landing trajectory. In order to simulate such trajectories, the first step is to derive the conditions for suitable LPOs. The derivation of Periodic Orbits[11,12] (POs) and Quasi-Periodic Orbits[13,14] (QPOs) in the CRTBP has been studied extensively in the past. The figure 5 below illustrates families of Lyapunov planar, vertical and Halo periodic orbits around the L1 and L2 Lagrangian Points of the Mars-Phobos system. However, such orbits are unstable and, as the dynamics is strongly perturbed, trying to remain on an LPO computed in the CRTBP would come at a significant station-keeping cost. The procedure used[8] is to *identify* LPOs in the Mars-Phobos-spacecraft CRTBP and then numerically continue a parameter that incrementally increases the effect of perturbations: the gravity harmonics and then the eccentricity. Eventually, families of POs, Quasi-halo and Lissajous QPOs are derived in the full MAG dynamics model. The invariant manifolds associated with all these orbits are then computed and those intersecting with Phobos are selected, as illustrated by the figure below.

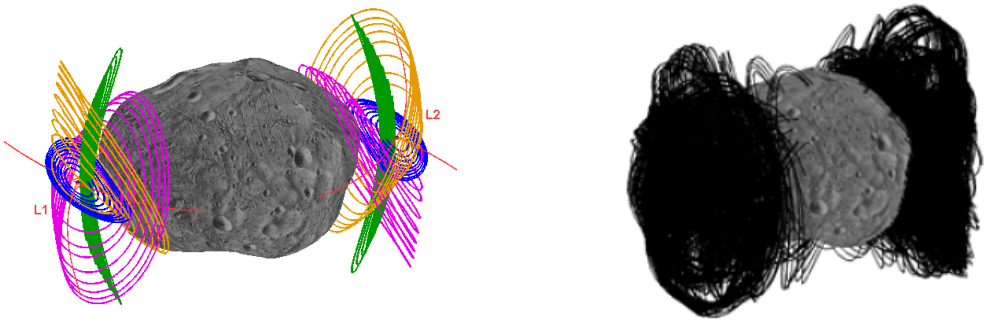

Figure 5. Families of L1 and L2 POs (left), and LPO manifolds interesecting Phobos (right)

If the landing site is not imposed, several trajectories are generally suitable candidates, and can be filtered according to an additional criterion. On the example considered, for each reachable landing site, the manifold with the highest incidence at touch-down (the most vertical) is selected. Finally the landing site is chosen as the one with the lowest touch-down velocity.

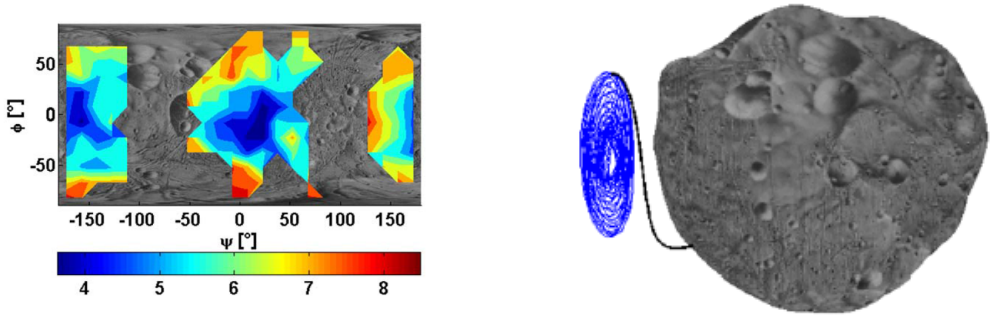

Figure 6. Touch-down velocity map (left) and selected manifold (right)

Soft landing manifold trajectory optimisation

The next step consists in implementing thrust to command the spacecraft to the landing site $\underline{r}_f$ with zero velocity $\underline{v}_f = 0$ at touch-down, as it would generally not be the case for a ballistic manifold.* The Open-Loop Guidance (OLG) profile is searched as a fixed order polynomial expression between $t_b > t_0$ and $t_f > t_b$, with time normalised by Phobos orbital period T.

$$\underline{U}(t > t_b) = \sum_{k=0}^{n} \underline{U}_k \left(\frac{t - t_b}{T} \right)^k \tag{5}$$

Such a fixed structure parametrisation of the OLG profile will lead to a suboptimal solution, but it has two important advantages: first, it is easy to implement in an on-board software, and besides it allows using parametric Nonlinear Programming (NLP) algorithms with a reduced set of parameters, for a faster optimisation process. The objective is to minimise the propulsive ΔV, while keeping an admissible level of error on the final state:

$$\min_{t_b, t_f, \{\underline{U}_k\}_{k \in [\![0,n]\!]}} J(t_b, t_f, \{\underline{U}_k\}_{k \in [\![0,n]\!]}) = \int_{t_0}^{t_f} \|\underline{U}(t)\| dt + \Psi \cdot \left(\underline{X}(t_f) - \underline{X}_f \right) \tag{6}$$

The parameter Ψ is a penalisation matrix on the final state error, and can be tuned so that the desired landing accuracy is achieved. The following figure illustrates a solution trajectory reached, using the ballistic manifold described in the previous section as the initial guess. Arrows represent the direction and relative magnitude of the optimal OLG propulsive acceleration.

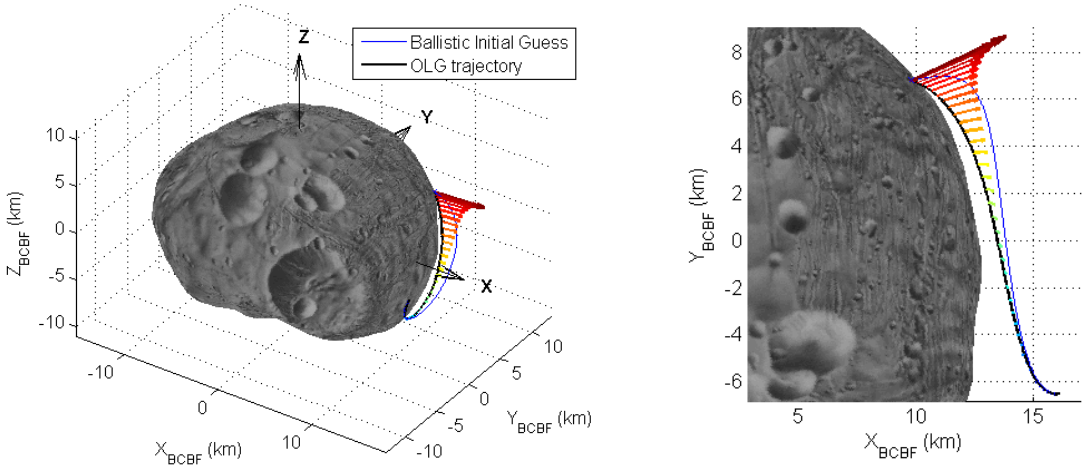

Figure 7. Optimised manifold landing trajectory

As is apparent on the previous plot, the thrusters are activated as soon as the spacecraft leaves the LPO. Local optima were reached by the optimiser with different values of $t_b > t_0$, when initialised with initial guesses far from t_0. However, as a general rule, and despite the fact that the thrust duration is less, the required propulsive acceleration is significantly increased, and its time integral, which corresponds to the propulsive ΔV, is increased as well.

*In the context of this work, no final free fall requirement has been considered for the derivation of the Open-Loop Guidance and subsequent closed-loop tests. This is without loss of generality as it would only modify the numerical values for the target position $\underline{r}_f$ and velocity $\underline{v}_f$, the free fall problem being addressed separately.

The next figures show the velocity profile, driven to 0 at the final time, compared to the initial guess ballistic trajectory, and the optimised command profile. The optimised open-loop soft landing has a duration of less than 2 hours and requires a propulsive ΔV of about 7 m/s.

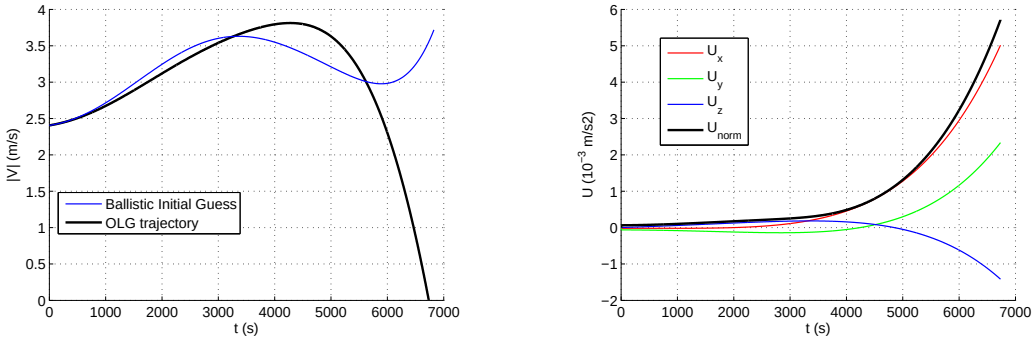

Figure 8. Optimised OLG manifold landing velocity (left) and command (right) profiles

Forced translation descent trajectory optimisation

In order to compare the manifold-based landing to a more classical approach, a second open-loop reference trajectory is computed as a forced translation from a hovering Station-Keeping (SK) point 10 km above the surface towards the same landing site, along the local normal to the surface.

This case is easier since a parametric analytical expression of the reference *kinematics* can be given so as to meet the soft landing requirement. The trajectory to follow is a straight line from the initial hovering position to the targeted landing site. However, the velocity profile to be followed by the spacecraft along this straight line can be optimised. Starting with a velocity equal to 0, and aiming for a zero velocity at the final time, a simple admissible solution is given by a trapezoidal profile: ramping up between t_0 and Δt_1 until the spacecraft reaches the maximum descent velocity v_d, then ramping down between $t_f - \Delta t_2$ and t_f to reach $v_f = 0$. This velocity profile can be described by only four parameters (Δt_1, Δt_2, v_d, t_f) that fully define the descent kinematics: by integration of this continuous piecewise function, one can derive the analytical expression of the position vector, with initial, final and continuity constraints used to derive the integration constants.

Table 3. Kinematics equations for the forced translation

Time interval	Position	Velocity	Total Acceleration
$t \in [t_0, \Delta t_1]$	$\underline{r}(t) = \underline{r}_0 + \frac{\underline{v}_d t^2}{2\Delta t_1}$	$\underline{v}(t) = \frac{\underline{v}_d t}{\Delta t_1}$	$\underline{a}(t) = \frac{\underline{v}_d}{\Delta t_1}$
$t \in [\Delta t_1, t_f - \Delta t_2]$	$\underline{r}(t) = \underline{r}_0 + \underline{v}_d \left(t - \frac{\Delta t_1}{2} \right)$	$\underline{v}(t) = \underline{v}_d$	$\underline{a}(t) = 0$
$t \in [t_f - \Delta t_2, t_f]$	$\underline{r}(t) = \underline{r}_f - \frac{\underline{v}_d (t_f - t)^2}{2\Delta t_2}$	$\underline{v}(t) = \frac{\underline{v}_d (t_f - t)}{\Delta t_2}$	$\underline{a}(t) = -\frac{\underline{v}_d}{\Delta t_2}$

An additional constraint is imposed by the continuity of the position of the spacecraft at $t = t_f - \Delta t_2$, reducing the number of free parameters down to three. This constraint is expressed as:

$$\underline{v}_d = \frac{\underline{r}_f - \underline{r}_0}{t_f - \left(\frac{\Delta t_1 + \Delta t_2}{2} \right)} \tag{7}$$

The propulsive acceleration required is obtained as the difference between the total acceleration and the apparent gravitational acceleration given by the MAG vector field velocity components:

$$\underline{U}(t) = \underline{a}(t) - f_v(\underline{X}, t) \tag{8}$$

This time the soft landing requirement is ensured by design, and the ΔV minimisation problem to solve can be written again as a parametric minimisation problem, with a single inequality:

$$\min_{\Delta t_1, \Delta t_2, t_f \geq \Delta t_1 + \Delta t_2} J(\Delta t_1, \Delta t_2, t_f) = \int_{t_0}^{t_f} \|\underline{U}(t)\| dt \tag{9}$$

The following figure illustrates the solution trajectory reached, the arrows representing the direction and relative magnitude of the optimal OLG propulsive acceleration.

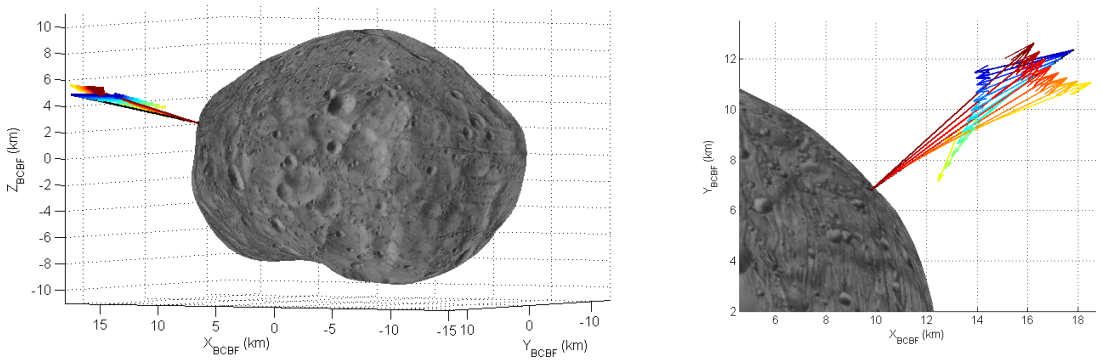

Figure 9. Optimised forced translation landing trajectory

The reached solution is such that the trapezoidal profile degenerates into a triangular profile with $\Delta t_1 + \Delta t_2 = t_f$ (active inequality constraint), as shown by the left figure below.

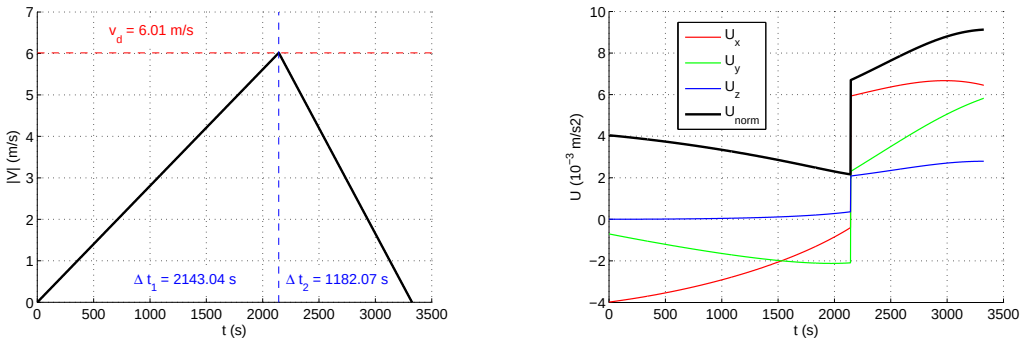

Figure 10. Optimised forced translation landing velocity (left) and command (right) profiles

The illustrated forced translation landing has a duration of less than 1 hour and requires a propulsive ΔV of about 16.5 m/s, which is significantly higher than the previous manifold-based trajectory. In addition, the hovering station-keeping point needs to be maintained prior to landing, at an average* cost of about 50 m/s per Phobos orbital period or 6.9 m/s per hour.

*The instantaneous SK cost depends on Phobos true anomaly, and the spacecraft's altitude, latitude and longitude.

CLOSED-LOOP GUIDANCE IMPLEMENTATION

In the previous section, open-loop command profiles (referred to as Open-Loop Guidance OLG) have been optimised and simulated in the dynamics environment described by the MAG model. As expected, when injected in an instance of the DKE model to simulate the *actual* dynamics experienced by the spacecraft, the OLG command profile generally steers the spacecraft on a trajectory that rapidly diverges from the nominal trajectory. The next figure illustrates the observed behaviour when simulating the manifold-based OLG in a Monte-Carlo campaign of 200 DKE runs with dispersed Phobos Gravity Harmonics. As evidenced by the left figure, some trajectories will actually crash on Phobos and some others will never reach its surface (single DKE realisation example on the right, with OLG command profile), demonstrating the importance of the considered perturbations on the dynamics, and calling for the implementation of robust closed-loop and guidance strategies.

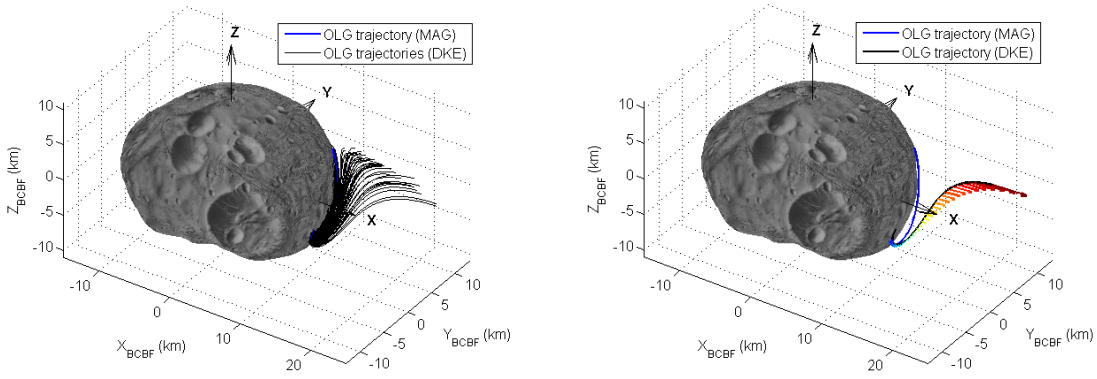

Figure 11. DKE simulations using the manifold landing trajectory OLG command profile

Guidance problem

The role of the *guidance* function is to compute, from the estimation of the current state of the spacecraft, the command and associated trajectory to follow so as to meet the mission's objectives, while respecting a given set of constraints and generally optimising a performance index. This function can be implemented either on the ground or directly in the on-board software, with a variety of possible intermediate architectures and subsequent impacts on the overall concept of operations. In the context of the present study, the objective is to maximise the autonomy of the spacecraft for the descent and landing phase: given the possibly long communication delays* as compared to the phase duration, the spacecraft should be able to complete its mission autonomously as soon as the descent is initiated.

Ideally, the guidance optimisation problem solved in real-time should be the same optimisation problem as the one considered for the mission analysis on the ground before the mission for the derivation of reference trajectories, only replacing the initial state by the actual (estimated) state at the current guidance step. Such an approach, sometimes called *fully explicit* Closed-Loop Guidance (CLG), is illustrated by the block-diagram below: in this case the pre-computed OLG profile is not used, or only to initialise the optimisation process. At the extreme opposite, a *fully implicit* strategy would use directly the OLG with no feedback of the estimated state to recalculate the command, which has been demonstrated to be inapplicable for our problem.

*Depending on the orbital configuration of the planets, round-trip communication times between the Earth and Mars can take from under 10 minutes up to more than 40 minutes.

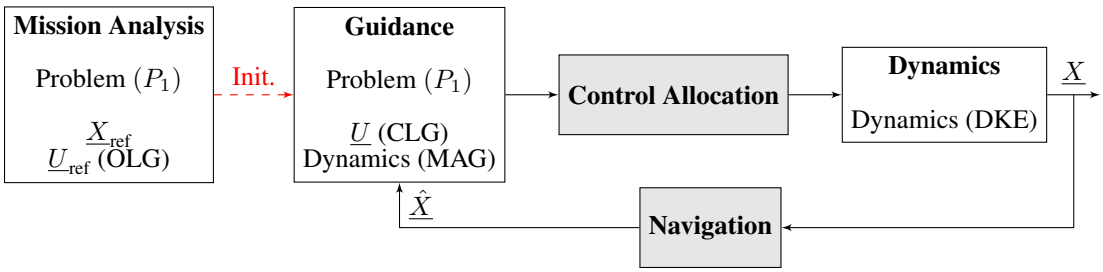

Figure 12. Fully explicit Closed-Loop Guidance (CLG) architecture*

In most cases however, the resolution of the full optimisation problem is not compatible with the on-board computational resources and/or time constraints, so that the guidance optimisation problem must be simplified. This simplification can arise from the description of the dynamics, the expression of the constraints, or even the selection of the performance index.

A typical example for a space trajectory guidance strategy is to use a quadratic performance index, instead of a more natural cost functional that would be associated with the propellant consumption. Let us consider two unconstrained optimisation problems (P_1) and (P_2), characterised by distinct cost functionals $J_{\mathcal{L}_1}$ and $J_{\mathcal{L}_2}$, defined respectively as the $\mathcal{L}_1$ and $\mathcal{L}_2$ norms of the control:

$$J_{\mathcal{L}_1}(\underline{U}) = \int_{t_0}^{t_f} \|\underline{U}(t)\| dt \quad ; \quad J_{\mathcal{L}_2}(\underline{U}) = \int_{t_0}^{t_f} \|\underline{U}\|^2(t) dt \tag{10}$$

The appendix provides a simple example of a dynamical system for which both problems can be solved analytically, minimising respectively $J_{\mathcal{L}_1}$ and $J_{\mathcal{L}_2}$, and illustrating some characteristic differences between the two corresponding types of solutions. For a realistic space trajectory optimisation problem, there is no such analytical solution, however in general:

- From a mission perspective, $\mathcal{L}_1$ is a more appropriate definition of the actuation cost: it is directly associated with the propulsive ΔV, and therefore the propellant consumption. Such problems are generally challenging to solve, characterised by non-smooth solutions†, requiring iterative and highly computationally demanding methods. Reference OLG in the previous sections have been derived using $\mathcal{L}_1$ cost functionals.
- Conversely, quadratic $(\mathcal{L}_2)$ optimisation problems are generally easier to solve numerically (smooth solutions) and in case the dynamics is simple, analytical solutions may even be found.

As a consequence, quadratic $(\mathcal{L}_2)$ optimisation problems are generally well adapted for on-board closed-loop guidance schemes, while minimum propellant consumption $\mathcal{L}_1$ optimisation problems are considered for the derivation of initial reference trajectories, part of the Mission Analysis commanding profile derivation calculated on the ground. However, as illustrated by the simple example in the appendix, penalties are expected to be incurred from the resolution by the guidance function of a distinct (easier) optimisation problem.

*The control allocation and navigation functions are not described in this paper, as they are very system-dependent: respectively on the propulsion system and thruster configuration, and the sensor suite and estimation algorithms, which are not the object of the study. In the full performance and robustness closed-loop simulation campaign, adequate performance models will be used for these two functions, to introduce additional sources of errors and delays.

†The fact that the solutions are singular does not mean that they are not achievable: saturated *bang-bang* like optimal control solutions may actually be more representative of the physical operating of a spacecraft propulsion system.

Guidance survey for autonomous planetary landing

Closed-loop guidance for autonomous landing has been the focus of several studies in the past twenty years. Most state-of-practice techniques provide simple analytical command laws, derived by considering highly simplified exogenous conditions, such as constant or time-explicit gravitational acceleration. Moreover, optimality is not always sought or achieved with respect to a quadratic performance index and no path constraint. Among these techniques are the following:

- The earliest, known as Proportional Navigation Guidance (PNG), inspired by the missile interception problem, aims at driving the Line-Of-Sight (LOS) rate to zero by applying an acceleration perpendicularly to the LOS direction $\underline{\Lambda}$ and proportional to the closing velocity V_c. Its expression contains a tunable parameter k known as the effective navigation ratio.[15]
- The Augmented PNG (APNG) variant accounts for the contribution of a constant gravity field, and the Biased PNG (BPNG) constrains the terminal LOS to $\underline{\Lambda}_f$.[16] The latter involves the *time-to-go* $t_{\text{go}} = t_f - t$, defined as the remaining duration until the end of the manoeuvre.
- Free (FTVG) and Constrained (CTVG) Terminal Velocity Guidance are solutions of a quadratic optimal control problem, with no path constraint, assuming a constant gravity $\underline{g}$.[17–19] These can be equivalently formulated in terms of *Zero Effort Miss* (ZEM) and *Zero Effort Velocity* (ZEV), respectively defined as the final errors in position and velocity if no command was to be applied after the current date:

$$\underline{ZEM}(t) = \underline{r}_f - \underline{r}(t_f)|_{\underline{U}(\tau\in[t,t_f])=\underline{0}} \;\; ; \;\; \underline{ZEV}(t) = \underline{v}_f - \underline{v}(t_f)|_{\underline{U}(\tau\in[t,t_f])=\underline{0}} \tag{11}$$

The analytical expressions for these guidance schemes are reported in the next table:

Table 4. Classical and optimal autonomous guidance schemes analytical expressions

Classical	Proportional Navigation Guidance (PNG)	$\underline{U} = kV_c\dot{\underline{\Lambda}}$
	Augmented PNG (APNG)	$\underline{U} = kV_c\dot{\underline{\Lambda}} - \frac{k}{2}\underline{g}_{\perp}$
	Biased PNG (BPNG)	$\underline{U} = 4V_c\dot{\underline{\Lambda}} - \underline{g} + \frac{2V_c}{t_{\text{go}}}(\underline{\Lambda} - \underline{\Lambda}_f)$
Optimal	Free Terminal Velocity Guidance (FTVG)	$\underline{U} = \frac{3}{t_{\text{go}}^2}(\underline{r}_f - \underline{r}) - \frac{3}{t_{\text{go}}}\underline{v} - \frac{3}{2}\underline{g}$
	Constrained Terminal Velocity Guidance (CTVG)	$\underline{U} = \frac{6}{t_{\text{go}}^2}(\underline{r}_f - \underline{r}) - \frac{4}{t_{\text{go}}}\underline{v} - \underline{g} - \frac{2}{t_{\text{go}}}\underline{v}_f$
	FTVG ZEM-ZEV formulation	$\underline{U} = \frac{3}{t_{\text{go}}^2}\underline{ZEM}$
	CTVG ZEM-ZEV formulation	$\underline{U} = \frac{6}{t_{\text{go}}^2}\underline{ZEM} - \frac{2}{t_{\text{go}}}\underline{ZEV}$

Guidance implementation and preliminary results

Among the above guidance schemes, the Constrained Terminal Velocity Guidance (CTVG) is the most appropriate as it results from an optimal control problem formulation with a fixed final *full* state, including the velocity. Its direct implementation in the closed-loop model including the *DKE* dynamics can be performed by taking at each guidance step t: the apparent gravitational acceleration given by the *MAG* vector field velocity components at the estimated current state $\underline{g} = f_v(\underline{\hat{X}}, t)$, and the remaining time until the end of the reference open-loop trajectory as the time-to-go.

Considering perfect navigation and actuation as well as a time-continuous closed-loop guidance correction, for a preliminary assessment in the best possible conditions, the trajectory meets the landing requirements, reaching the target at zero velocity with a good accuracy. However, the results exhibit some significant limitations associated with this direct implementation:

- The impossibility to include some path constraints on the trajectory implies that it is not possible to prevent trajectories that would theoretically reach the desired final state with intermediate positions passing below the surface of Phobos, actually leading to a crash.

- As foreseen in the previous paragraph and illustrated in the appendix, the ΔV required to follow the closed-loop trajectory is significantly increased as compared to the OLG reference.

The next figure illustrates such an example, starting from the initial conditions of the manifold-based trajectory, but following a very different path and crashing into Phobos. The theoretical ΔV until the final state is reached is 15.4 m/s, which is more than twice the ΔV of the reference OLG.*

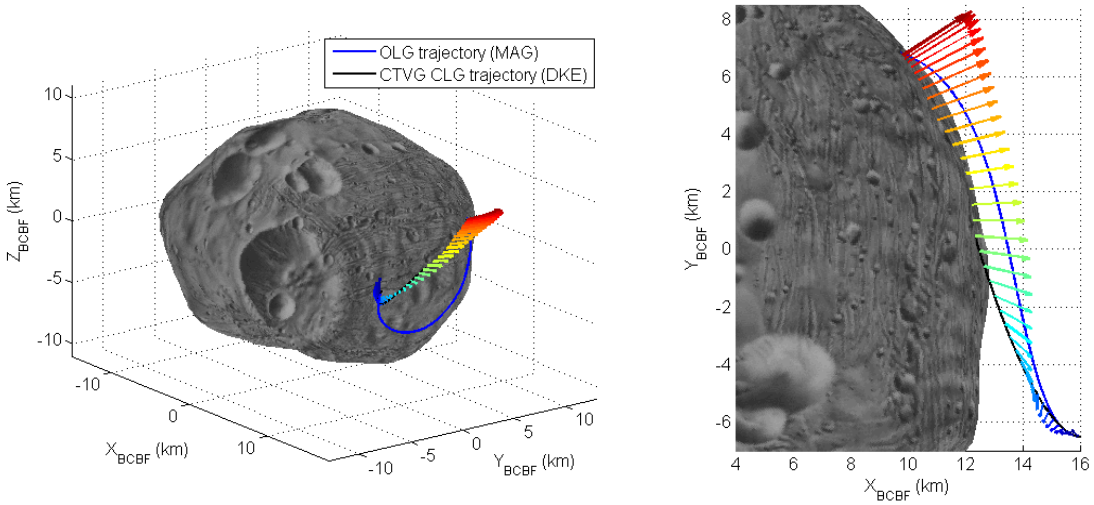

Figure 13. Crashing trajectory with CTVG simplified explicit closed-loop guidance DKE simulation

Both limitations can be addressed by an adaptation of the guidance strategy, illustrated by the next figure. Instead of targeting at each *guidance step* the *final* reference date and state (landing site with zero-velocity), the time-to-go, or *guidance horizon* (between the current date and the target guidance date), can be reduced to target an intermediary state interpolated on the reference trajectory.

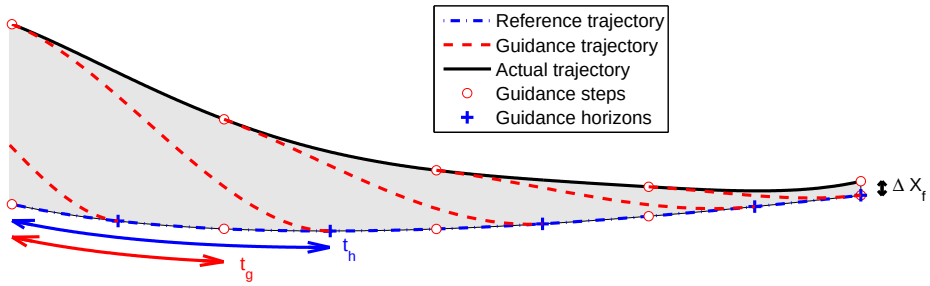

Figure 14. Way-point based CTVG schematic principle

*In the CTVG problem formulation, the final time t_f is fixed, so that a one-dimensional optimisation (line search) of this parameter could be envisaged as part of the guidance command update. However this would lead to consider again an iterative algorithm that was avoided by using an analytical solution of a pre-solved problem.

A parametric analysis of this strategy has been performed for a range of *guidance steps* t_g and *guidance horizons* $t_h \geq t_g$, still assuming perfect navigation and actuation to focus on the guidance. The CTVG trajectory illustrated earlier then becomes a special case of this generalised *way-point based* CTVG algorithm, with a guidance horizon equal to the full time-to-go until landing and a continuous guidance correction of the trajectory. The accuracy can be measured by the 2-norm of a vector defined by the (normalised) error on the position and velocity at the nominal final time t_f.*

$$J(\Delta r_f, \Delta v_f) = \left\| \left(\frac{\Delta r_f}{\Delta r_{\text{tol}}}, \frac{\Delta v_f}{\Delta v_{\text{tol}}} \right) \right\|_2 = \sqrt{\left(\frac{\Delta r_f}{\Delta r_{\text{tol}}} \right)^2 + \left(\frac{\Delta v_f}{\Delta v_{\text{tol}}} \right)^2} \tag{12}$$

Results are presented for $t_g \in [10,\ 600]$ s, $t_h \in [t_g,\ t_f]$, $\Delta r_{\text{tol}} = 10$ m and $\Delta v_{\text{tol}} = 10$ cm/s, on a single instance of the DKE dynamics model (used in the previous simulation).

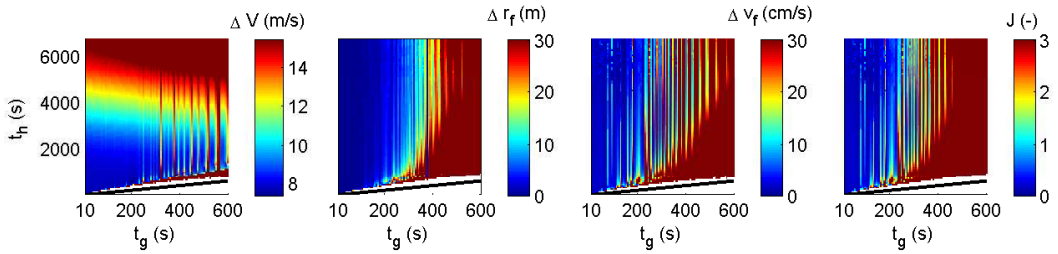

Figure 15. Propulsive ΔV (left), errors in position, velocity and J index at time t_f (right)

A few points on the (t_g, t_h) domain have been selected for further analysis, to derive some statistics (mean value and standard deviation) for the the propulsive ΔV and final accuracy, drawn from a Monte-Carlo analysis on the DKE model realisations, and reported in the next tables.

Table 5. Parametric performance analysis of the way-point based CTVG - Statistical DKE

$\mu[\Delta V]$ (m/s)		t_g (s)			
		10	100	200	400
t_h (s)	1000	7.34	7.36	7.36	7.66
	2000	8.07	8.16	8.23	8.39
	3000	9.91	10.1	10.3	10.9

$\sigma[\Delta V]$ (m/s)		t_g (s)			
		10	100	200	400
t_h (s)	1000	0.96	0.96	0.95	1.10
	2000	1.05	1.08	1.12	1.08
	3000	1.13	1.17	1.23	1.27

$\mu[J]$ (-)		t_g (s)			
		10	100	200	400
t_h (s)	1000	0.17	0.55	0.68	4.71
	2000	0.15	0.52	0.51	4.63
	3000	0.13	0.45	0.53	5.55

$\sigma[J]$ (-)		t_g (s)			
		10	100	200	400
t_h (s)	1000	0.09	0.26	0.57	2.04
	2000	0.09	0.39	0.41	2.81
	3000	0.09	0.32	0.39	3.71

As could be expected, this analysis shows that the guidance performance is increased for a higher correction frequency (small t_g), which in practice will be limited by the on-board computational time and the delays involved in the overall closed-loop. Regarding the tuning of the guidance horizon, shorter times for $t_h > t_g$ are better for the ΔV, almost asymptotically reaching the reference OLG ΔV, with a lesser impact on the final accuracy, up to a certain limit when the closed-loop actually becomes unstable and the trajectories rapidly diverge from the reference.

*While the state errors at time t_f and the derived J performance index do indeed measure the *guidance* performance as a deviation from the nominal target in state and time, it is not necessarily representative of actual trajectories, as some will have crashed before t_f, and some others may very well reach the surface of Phobos at a later date.

CONCLUSION AND FUTURE WORK

This paper presented the current status of the work conducted by Airbus Defence and Space and the University of Bristol on strategies for autonomous landing on small bodies, with a focus on the mission analysis, reference trajectory optimisation, and preliminary closed-loop guidance assessment. In the challenging framework of a landing on Phobos, Libration Point Orbits have been computed and proposed to be used as natural observation platforms, while their associated manifolds serve as initial guess for optimising a controlled landing trajectory towards a selected landing site. Owing to limited on-board resources, the guidance function will have to solve a simpler optimisation problem, at the expense of an increased propellant consumption. This can however be mitigated by making the most of the reference trajectory in a way-point based adaptation of quadratic optimal guidance schemes. Overall, the strategy proved to be compliant with the surface access requirements, and to cope with highly complex and uncertain dynamics environments, achieving a significant reduction of the propellant consumption when compared to more classical approaches.

Started in mid-2016, the project is still ongoing as the present paper is being redacted. A proper performance and robustness assessment of the closed-loop GNC subsystem must include realistic performance models for the navigation and actuation functions, not presented in this paper. In addition to the errors associated with these (error in the estimation of the current state, thruster misalignments, and errors in the realisation of the boosts), delays are to be expected, and both will alter the propellant consumption and landing accuracy. The solution currently baselined for Phobos-relative navigation relies on an hybridisation of Vision-Based Navigation (VBN) and radar altimeter measurements to improve the poor range observability achievable by vision-only: the Image Processing (IP) in particular is likely to be one of the most time demanding operations. Importantly for the reference trajectory optimisation, further constraints could also be proved to be required for the trajectory to be navigable (e.g. requiring a more vertical final landing trajectory).

Future work includes the investigation of augmented guidance strategies specifically aimed at addressing *robustness*, including results from the nonlinear sliding mode control theory, recently assessed in asteroid landing scenarios.[20,21] Finally, the reformulation of the guidance problem as a tracking-like problem opens the door for a range of control theory applications. By implementing an inner control loop of a linearised model of the dynamics in the vicinity of the reference trajectory, as shown schematically in the next block-diagram, several techniques for the synthesis, tuning and analysis from modern robust control theory become applicable. These include in particular H_∞[22] methods, used in past space missions with success on robust attitude control problems, while uncertainties can be modelled as time-invariant Linear Fractional Transformations (LFT),[23] capturing time-varying effects via Linear Parameter-Varying (LPV) models.[24]

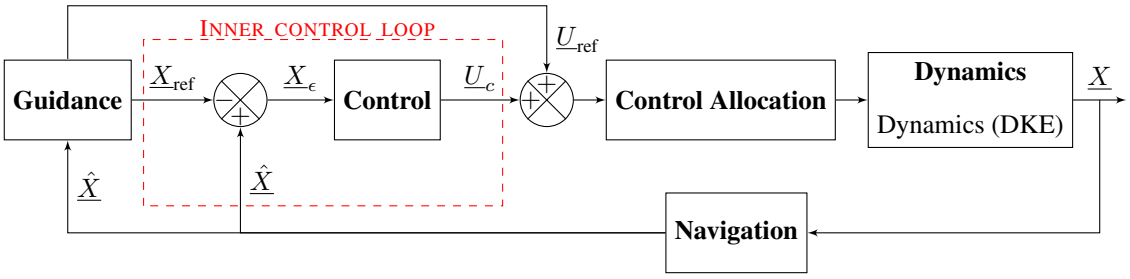

Figure 16. Closed-Loop architecture with control inner loop

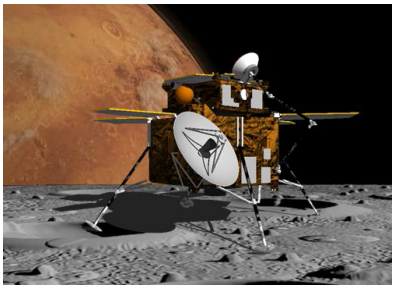

Figure 17. Colour composite of Phobos taken by ExoMars TGO in November 2016 (left) [Credits: ESA/Roscosmos/CaSSIS] and artist's view of a Phobos Lander (right)

ACKNOWLEDGEMENT

This work has been funded by the UK Space Agency (UKSA), under the National Space Technology Programme (NSTP). The authors are thankful to Mick Johnson and Christopher Brownsword, respectively Director and Technical Director of the Centre for Earth Observation and Instrumentation (CEOI), for their support and collaboration in the first months of the project, as well as Barbara Richardson, NSTP Programme Manager and coordinating the project for the UKSA.

NOTATION

μ_g	Gravity constant = GM
U_g	Gravity field scalar potential
r	Orbital radius (wrt Phobos)
θ	Co-latitude
ϕ	Longitude
$C_{n,m}$, $S_{n,m}$	Cosinus and Sinus Gravity Harmonics coefficients
$\mu[A]$	Mean value (of a random variable A)
$\sigma[A]$	Standard deviation (of a random variable A)
$\mathcal{N}(\mu, \sigma)$	Gaussian distribution with mean μ and standard deviation σ
$\underline{X}$	State vector: position and velocity relative to Phobos BCBF
$f(\underline{X}, t)$	Dynamics vector field (MAG or DKE)
e	Phobos orbit eccentricity
n	Phobos orbit mean motion
T	Phobos orbital period
ν	Phobos true anomaly
$\underline{r}$	Spacecraft position (Phobos BCBF)
$\underline{v}$	Spacecraft velocity (Phobos BCBF)
$\underline{a}$	Spacecraft acceleration (Phobos BCBF)
$\underline{U}$	Command vector: propulsive acceleration
k	Effective navigation ratio (PNG guidance algorithm)
$\underline{\Lambda}$	Line-Of-Sight (LOS) vector
V_c	Closing velocity (relative to the target)
t_{go}	Time-to-go
$\underline{ZEM}$	Zero-Effort-Miss
$\underline{ZEV}$	Zero-Effort-Velocity

APPENDIX: $\mathcal{L}_1$ VERSUS $\mathcal{L}_2$ OPTIMAL CONTROL DOUBLE INTEGRATOR EXAMPLE

In this appendix, the difference between $\mathcal{L}_1$ and $\mathcal{L}_2$ optimal control problems is illustrated on the double integrator archetypal example of a normalised mechanical system, with bounded control:

$$\dot{\underline{X}} = f(\underline{X}, \underline{U}) \text{ , with } \begin{cases} \underline{X} & = & [x_1, x_2]^T \\ \underline{U} & = & u \in [-u_{max}, +u_{max}] \\ f(\underline{X}, \underline{U}) & = & [x_2, u]^T \end{cases} \tag{13}$$

In this example, x_1 is the scalar position of the system, $x_2 = \dot{x_1}$ is the velocity, and the acceleration $\ddot{x_1}$ is directly equal to the input command u that drives the system. For a standard *rendezvous* problem with zero initial (and final) velocity with fixed terminal time t_f, we must have in addition:

$$\underline{X}(t_0) = [a, 0]^T \quad ; \quad \underline{X}(t_f) = [b, 0]^T \tag{14}$$

We consider two unconstrained optimisation problems (P_1) and (P_2), characterised by distinct cost functionals $J_{\mathcal{L}_1}$ and $J_{\mathcal{L}_2}$, defined respectively as the $\mathcal{L}_1$ and $\mathcal{L}_2$ norms of the control function:

$$(P_1) \quad : \quad J_{\mathcal{L}_1}(u) = \int_{t_0}^{t_f} |u(t)| dt \quad ; \quad (P_2) \quad : \quad J_{\mathcal{L}_2}(u) = \int_{t_0}^{t_f} u^2(t) dt \tag{15}$$

The advantage of the simple dynamical system considered is that analytical solutions can be derived for both optimal control problems, illustrated below for $u_{max} = 1$, $t_f = 10$, $a = 0$, $b = 10$.

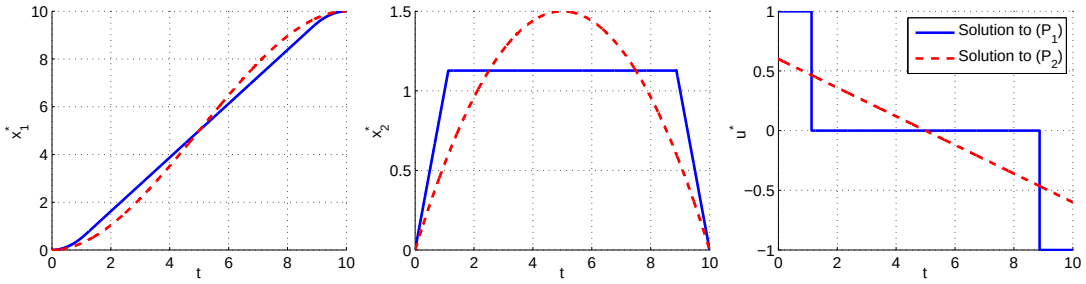

Figure 18. Optimal position $x_1{}^*$, velocity $x_2{}^*$ and command u^* profiles for problems (P_1) and (P_2)

As evidenced by the next table, controls $u^*{}_{\mathcal{L}_1}$ and $u^*{}_{\mathcal{L}_2}$ are only optimal for their respective problems, the solution of (P_1) (resp. (P_2)) minimising the cost functional $J_{\mathcal{L}_1}$ (resp. $J_{\mathcal{L}_2}$).

Table 6. $\mathcal{L}_1$ and $\mathcal{L}_2$ costs of (P_1) and (P_2) solutions

Problem	Optimal control	Functional $J_{\mathcal{L}_1}$	Functional $J_{\mathcal{L}_2}$
(P_1)	$u^*{}_{\mathcal{L}_1}$	**2.25**	2.25
(P_2)	$u^*{}_{\mathcal{L}_2}$	3.00	**1.20**

This example illustrates some fundamental differences between $L1$ and $L2$ categories of optimal control problems, with a smooth solution for the quadratic problem, and a discontinuous *bang-bang* solution for the $L1$ problem: to the limit where $u_{max} \to \infty$ (unbounded control), L1 optimal control would tend to a couple of symmetric Dirac distributions at t_0 and t_f, corresponding to the model of impulsive (instantaneous) velocity increments, and asymptotic cost $J_{\mathcal{L}_1} = 2(b-a)/t_f = 2.00$.

REFERENCES

[1] Z. Junjun, N. Dauphas, A. Davis, I. Leya, and A. Fedkin, "The proto-Earth as a significant source of lunar material.," *Nature Geoscience*, Vol. 5, No. 4, 2012, pp. 251 – 255.

[2] L. Peacocke, M. C. Perkinson, J. Reed, M. Wolf, T. Lutz, and C. Balemboy, "Terminal Descent and Landing Architectures for a Mars Precision Lander," *8th International Planetary Probe Workshop*, 2011.

[3] L. Peacocke, S. Kemble, M. Chapuy, and H. Scheer, "MarcoPolo-R: Mission and Spacecraft Design," *European Planetary Science Congress 2013*, Vol. 8, Sept. 2013, pp. EPSC2013–116.

[4] S. Barraclough, A. Ratcliffe, R. Buchwald, H. Scheer, M. Chapuy, M. Garland, and D. Rebuffat, "Phootprint: A European Phobos Sample Return Mission," *11th International Planetary Probe Workshop*, Vol. 1795 of *LPI Contributions*, June 2014, p. 8030.

[5] T. Duxbury and J. Callahan, "Pole and prime meridian expressions for Phobos and Deimos.," *Astronomical Journal*, Vol. 86, No. 11, 1981, pp. 1722 – 1727.

[6] V. Szebehely, *Theory of orbit : The restricted problem of three Bodies.* Academic Press, 2012.

[7] M. Zamaro and J. D. Biggs, "Identification of new orbits to enable future mission opportunities for the human exploration of the Martian moon Phobos.," *Acta Astronautica*, Vol. 119, 2016, pp. 160 – 182.

[8] M. Zamaro and J. D. Biggs, "Dynamical Systems Techniques for Designing Libration Point Orbits in Proximity of Highly-Inhomogeneous Planetary Satellites: Application to the Mars-Phobos Elliptic Three-Body Problem with Additional Gravity Harmonics.," *AIP Conference Proceedings*, Vol. 1637, No. 1, 2014, pp. 1228 – 1240.

[9] B. F. Chao and D. P. Rubincam, "The gravitational field of Phobos," *Geophysical Research Letters*, Vol. 16, No. 8, 1989, pp. 859–862, 10.1029/GL016i008p00859.

[10] M. Zamaro, *Natural and artificial orbits around the Martian moon Phobos*. PhD thesis, University of Strathclyde, 10 2015.

[11] R. Farquhar, "The control and use of libration-point satellites.," 1968, p. 214.

[12] K. Howell, "Three-dimensional, periodic, 'halo' orbits.," *Celestial Mechanics*, Vol. 32, No. 1, 1984, pp. 53 – 71.

[13] J. M. Mondelo González and G. Gómez, "The dynamics around the collinear equilibrium points of the RTBP.," 2001.

[14] E. Kolemen, N. Kasdin, and P. Gurfil, "Multiple Poincare sections method for finding the quasiperiodic orbits of the restricted three body problem.," *Celestial Mechanics and Dynamical Astronomy*, Vol. 112, No. 1, 2012, pp. 47 – 74.

[15] P. Zarchan, *Tactical and strategic missile guidance.* 4th, n.d.

[16] K. Byung Soo, L. Jang Gyu, and H. Hyung Seok, "Biased PNG law for impact with angular constraint.," *IEEE Transactions on Aerospace and Electronic Systems*, Vol. 34, No. 1, 1998, pp. 277 – 288.

[17] M. Hawkins, Y. Guo, and B. Wie, "ZEM/ZEV Feedback Guidance Application to Fuel-Efficient Orbital Maneuvers Around an Irregular-Shaped Asteroid.," *Papers - American Institute of Aeronautics and Astronautics*, Vol. 7 of *AIAA guidance, navigation, and control conference*, 2012, pp. 5745 – 5768.

[18] G. Yanning, M. Hawkins, and W. Bong, "Applications of Generalized Zero-Effort-Miss/Zero-Effort-Velocity Feedback Guidance Algorithm.," *Journal of Guidance, Control, and Dynamics*, Vol. 36, No. 3, 2013, pp. 810 – 820.

[19] M. Hawkins, Y. Guo, and B. Wie, "Guidance Algorithms for Asteroid Intercept Missions with Precision Targeting Requirements (AAS 11-531).," *Advances in the Astronautical Sciences*, Vol. 142, 2012, pp. 1951 – 1970.

[20] R. Furfaro, B. Gaudet, D. Wibben, and J. Simo, "Development of Non-Linear Guidance Algorithms for Asteroids Close-Proximity Operations.," University of Arizona, Tucson, AZ, USA, 8041, 2013.

[21] R. Furfaro, D. Cersosimo, and D. Wibben, "Asteroid Precision Landing via Multiple Sliding Surfaces Guidance Techniques.," *Journal of Guidance, Control, and Dynamics*, Vol. 36, No. 4, 2013, pp. 1075 – 1092.

[22] A. Falcoz, C. Pittet, S. Bennani, A. Guignard, C. Bayart, and B. Frapard, "Systematic design methods of robust and structured controllers for satellites.," *CEAS Space Journal*, Vol. 7, No. 3, 2015, pp. 319 – 334.

[23] J. Doyle, A. Packard, and K. Zhou, "Review of LFTs, LMIs, and mu.," Dept. of Electr. Eng., Caltech, Pasadena, CA, USA, 1991.

[24] A. Marcos and S. Bennani, "LPV Modeling, Analysis and Design in Space Systems: Rationale, Objectives and Limitations.," *Papers - American Institute of Aeronautics and Astronautics*, Vol. 1 of *Guidance, navigation and control*, 2009, pp. 286 – 308.